# Characterization of integrated heaters for ultra-long waveguides

Ang Li, 1,2,\* D Qixiang Cheng, 3 D and Yeshaiahu Fainman 4

**Abstract:** The demand for ultra-long waveguides with tunable refractive index keeps growing in various applications, such as tunable delay line, Fourier transform spectrometers, microwave filters, signal processors, programmable photonics circuits, Lidar etc. Thermal tuning using integrated heaters is so far the most popular option to modulate the waveguide index due to simplicity of fabrication, high tuning efficiency, wide tuning range as well as absence of spurious amplitude modulation. But for ultra-long waveguide, the heater design needs to take the in-plane geometry into consideration in order to optimize particular performance metrics. Therefore, in this manuscript we report both theoretical modelling and experimental characterization of integrated heaters for ultra-long waveguides that pays special attention to the impacts of heater geometry.

© 2022 Optica Publishing Group under the terms of the Optica Open Access Publishing Agreement

#### 1. Introduction

One crucial promotion for the prosperity of silicon photonics should be attributed to its ease of index modulation though various methods, as numerous devices or circuits function relying upon dynamic index modulation, covering applications in sensing, communications, Lidar, microwave photonics, optical logic, laser cavities etc [1–11]. Among different index modulation methods such as plasma dispersion effect by doping silicon waveguides, employing materials that exhibit efficient electro-optic effects as cladding and so on, thermal tuning using integrated heaters is probably the most popular choice thanks to the high thermo-optic coefficient of silicon ( $1.8 \times 10^{-4}$  /K), ease of fabrication, no spurious amplitude modulation and negligible loss induced to the light in silicon waveguides. So far, most demonstrations of silicon photonics with thermal tuning do not require particular in-plane geometric design and optimization of heaters, as they are mainly for short waveguides (up to 1mm) [12–16]. The heater design would then be straightforward and simple: make the heater co-propagate with the waveguide underneath with correct choice of the distance between heater and waveguide core.

While on the other hand, with the maturation of fabrication technology, the propagation loss of waveguide keeps decreasing and applications where ultra-long waveguides play a key part start to grow rapidly, like microwave filter and signal processors that require a few mm long cavity in order to get GHz frequency selectivity or centimeter long for sub-GHz selectivity [3,7,17]; programmable optical processor where the interconnect could be easily over 1 cm [1,2,5,18], as an example, in [2], the programmed ring cavity could have a length over 14cm; compact spectrometers relying upon long waveguide with tunable refractive index in order to deliver high spectral resolution [8]; silicon photonics gyroscopes with centimeter long waveguide to get high sensitivity [19]; tunable delay line that contains ultra-long waveguide [6] etc. Usually, it is desirable or necessary for the long waveguides in applications mentioned above to enjoy

#468845 Journal © 2022 https://doi.org/10.1364/OPTCON.468845

<sup>&</sup>lt;sup>1</sup>Key Laboratory of Radar Imaging and Microwave Photonics, Ministry of Education, Nanjing University of Aeronautics and Astronautics, Nanjing 210016, China

<sup>&</sup>lt;sup>2</sup>Littin Tech Co., Ltd., Jiangsu, China

<sup>&</sup>lt;sup>3</sup>Department of Engineering, University of Cambridge, 9 JJ Thomson Avenue, Cambridge CB3 0FA, UK

<sup>&</sup>lt;sup>4</sup>Department of Electrical and Computer Engineering, University of California at San Diego, La Jolla, CA 92093-0407, USA

<sup>&</sup>lt;sup>\*</sup>ang.li@nuaa.edu.cn

thermal tuning as other index modulation methods like free carrier plasma modulator becomes non-trivial to be implemented for ultra-long waveguides. Then the heater to drive those ultra-long waveguides would become non-trivial to design because it is unfeasible to make the heater follow the same routine as the waveguide otherwise the heater would end up with huge resistance and the total footprint would be unacceptably large. Moreover, the metric for characterizing performance of short heater mainly lies in the power efficiency  $P_{\pi}$ , namely how much power is needed to get a phase change of  $\pi$ . While for ultra-long heaters, depending on specific applications, the requirement on the heater performance might be varying. For instance, for applications like spectrometer, the primary concern is the maximum phase change that could be achieved within certain voltage, as for such a device, the spectral resolution directly depends on the maximum achieved phase change and typically the associated power source to drive the heater has a limit on the max output voltage. While for other applications like microwave filters, the power efficiency might go with higher priority. What's more, the modeling for short and long heater also shows a discrepancy: for short heater and waveguide, where both have the same length, the temperature change  $\Delta T$  is simply modelled to be proportional to the power dissipation of the heater P and power efficiency  $P_{\pi}$  is believed to be independent on waveguide and heater length. While for long heater, we will show later that the model becomes inaccurate and needs to be modified to take heater geometry and waveguide length into consideration.

In this paper, we provide a simple theoretical model to describe the performance of ultra-long heaters and experimentally characterize a method to design heaters for 10 cm long waveguide that maintains compact footprint, full coverage of waveguide, low resistance, moderate power efficiency and fast response time. We also compare the performance of varying heaters using the same design method with focus on power efficiency, maximum phase change under constant voltage source, thermal nonlinearities and time response, respectively. Note that, there are various materials for thermal tuning such as metal, graphene, doped silicon and polysilicon [12,20–22]. But the model presented below is independent on the material as long as correct material constants are considered in the model.

#### 2. Design and model

When the waveguide is longer than 1~mm, it's beneficial to have a serpentine shape that drastically reduces the footprint as shown in Fig. 1(a). For such a waveguide, the heater could not simply propagate along the waveguide as it would end up with huge resistance that is hard to be driven by common dc source and a considerable footprint due to the large metal wire width and large minimum gap between adjacent parallel metal wires. A design that allows the heater to have compact footprint, low total resistance, full coverage of the waveguide as well as high power efficiency is needed. So we propose to design heater in the way shown in Fig. 1(b). The heater is broadened to cover multiple waveguide cores to ensure full coverage of the waveguide as well as retain compact footprint. With increasing heater width, the length of the heater would also decrease accordingly for a given waveguide. The border-to-border gap between two waveguides should be at least 2 um to avoid unwanted cross-talk. Then the main design freedom for such a structure is the number of waveguide cores N to be covered by one heater. And we will show later than varying N would lead to very different heater performance.

An analytic model is developed to predict the heater performance. Take a cubic heater with unit length dL as an example (shown in Fig. 2), according to Fourier's Law for heat conduction [23,24], the temperature change  $\Delta T$  induced by the amount of power dissipation P through a resistive element with absolute thermal resistance  $R_h$  is:

$$\Delta T = R_h P, \ R_h = \frac{h r_h}{W dL} = \frac{h}{k_h W dL} \tag{1}$$

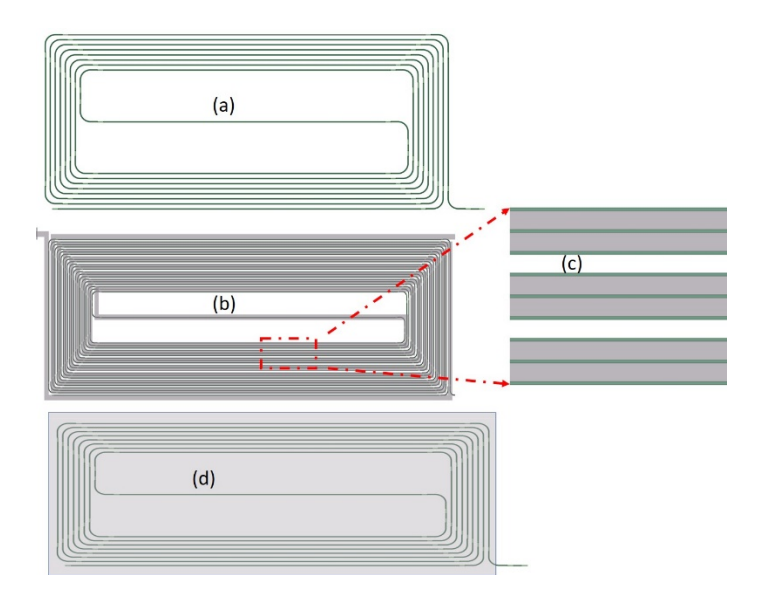


**Fig. 1.** Schematics of the serpentine waveguide alone colored in green (a) and waveguide with top heater plotted in grey (b). (c) shows the zoomed top-view of the heater covering a couple of waveguide cores. (d) presents an extreme case where the entire serpentine waveguide is covered by a rectangular heater.

where  $r_h$  and  $k_h$  refer to the thermal resistivity and thermal conductivity respectively and they are material constants that are independent of the heater geometry. The thickness is usually pre-defined by the foundry as well and thus doesn't belong to geometric design of the heater. Then define the sheet resistance of a heater  $R_{\blacksquare}$ , which is another material constant of the heater. The unit-length resistance dR and total resistance R is:

$$dR = R_{\blacksquare} \frac{dL}{W}, \ R = R_{\blacksquare} \frac{L}{W}$$
 (2)

where L and W represents the heater length and width, respectively. A voltage V is applied to the heater and the current flowing through each unit-length is  $I = \frac{V}{R} = \frac{VW}{LR_{\blacksquare}}$ . Then the power dissipation by the unit-length heater is  $dP = I^2 dR = \frac{V^2 W}{R_{\blacksquare} L} dL$ . The local temperature change caused by power dissipation of the unit-length heater is defined as:

$$\Delta T = \frac{hr_h}{WdL}dP = \frac{hr_h}{R_{\blacksquare}} \frac{V^2}{L^2} = hr_h \frac{P}{WL}$$
 (3)

Here, P is the total power dissipation of the entire heater. These equations suggest that the temperature change drops with the square of heater length when we consider constant voltage and drops with the product of width and length if we consider constant total power consumption. Then the total phase change along the waveguide is:

$$\Delta \varphi \propto L_w k_n \Delta T = \frac{k_n h r_h}{R - L_w^2} V^2 = k_n h r_h \frac{L_w}{WL} P \tag{4}$$

where  $L_w$  is the waveguide length and  $k_n = \frac{\partial n}{\partial T}$  is a coefficient relating waveguide index change with temperature change, which is another constant depending on the waveguide material. For silicon it could be approximated to  $1.8 \times 10^{-4}$ . This equation shows the maximum phase change as a function of voltage and total power consumption, respectively. In the case of fixed waveguide

length  $L_w$ , if the primary concern is the largest achievable phase change within certain voltage, then the term  $\frac{1}{L^2}$  should be maximized. The heater width doesn't play a role here. This could be done by increasing N. While if the power efficiency comes with higher priority, then the term  $\frac{1}{WL}$  should be increased accordingly. Now both the heater width and length should be reduced in order for higher power efficiency, this is difficult to achieve as we still need full coverage of the waveguide by the heater. Increasing N would lead to an increase of W and decrease of L, but generally speaking, it would lead to a larger product of WL as now the heater covers more area. If the waveguide length  $L_w$  is also a design freedom, then it suggests this device could lead to higher power efficiency than conventional design, where the waveguide and heater have the same length as  $\frac{L_w}{I}$  could be much larger than 1.

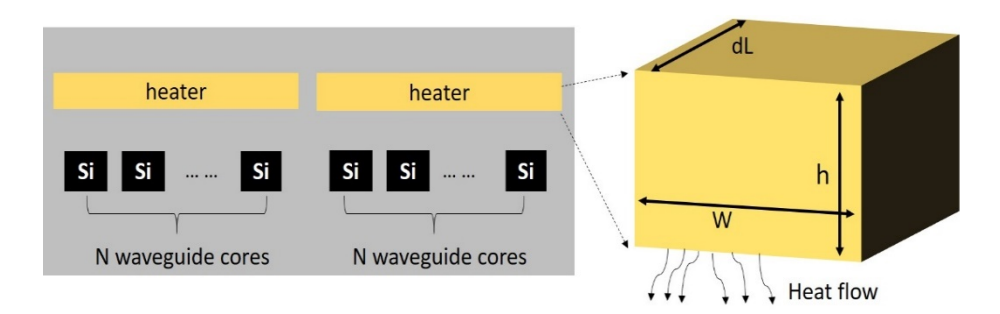
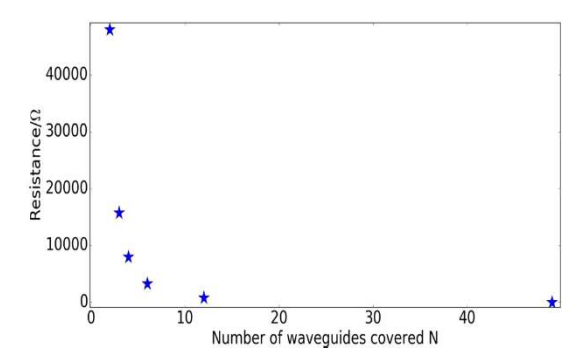


**Fig. 2.** Cross-section of the structure and a graphic model for the heater with unit length dL. The number of waveguide cores that are covered by a heater (N) is the design freedom we'd like to investigate. The thickness of the heater is noted with h and the cross-section that is perpendicular to the heat flow has an area of WdL.

To verify this, we design and fabricated 6 MZIs that have balanced serpentine waveguides with different N. The first 5 have N = 2,3,4,6,12, respectively, while the 6th MZI is an extreme case that the entire serpentine waveguide is simply covered by a rectangular heater (N = 49, as plotted in Fig. 1(d)) is also fabricated. For all devices, the waveguide has a length of 87.3 mm, width of 0.5um and a border-to-border gap between adjacent waveguides of 3um, thus they have the same footprint.

#### 3. Experimental results

The devices were fabricated on a 220 nm thick silicon-on-insulator wafer with 1.6 um top oxide cladding at Applied Nanotools. The lithography is done using electron beam thus introduce negligible fabrication variation between two arms and heaters. Grating couplers with center wavelength at 1540~nm are employed for the fiber/chip coupling. The resistive element of the heater is 200 nm thick titanium-tungsten alloy with sheet resistance of  $R_{\blacksquare}=4\Omega/\text{sq}$ . There is another protection layer of silicon dioxide on top of the heater. The dimensions and measured resistance of the 6 different heaters are given in Fig. 3. To study the heater performance, we fix the input wavelength@1540 nm (peak wavelength of our grating couplers) and measure the device output by sweeping power injection to the heaters. The results are plotted in Fig. 4 with x-axis being electrical power and voltage respectively. For the plots showing output vs voltage applied to the heater, it is quite clear that increasing N would efficiently lead to more phase change within same amount of voltage. The way we compare them is to check the required voltage for ten  $2\pi$ phase change (10 periods). When N = 49, it only requires less than 3 V to get this amount of phase change, while the value grows to 12 V for N = 12, 22 V when N = 6, and as large as 90 V when N = 2. Therefore, for applications that requires large phase change within limited voltage source, like Fourier transform spectrometer [8], it's desired to design the heater with large N.



N	L/mm	W/um	R/ohm
2	45	4	47.7k
3	30.3	7.5	15.8k
4	23.2	11	8.8k
6	16.1	17.5	3.3k
12	8.9	39.1	0.8k
49	2	220	40

 $\textbf{Fig. 3.} \ \ Dimensions \ and \ measured \ resistance \ of \ these \ heaters \ with \ different \ N.$ 

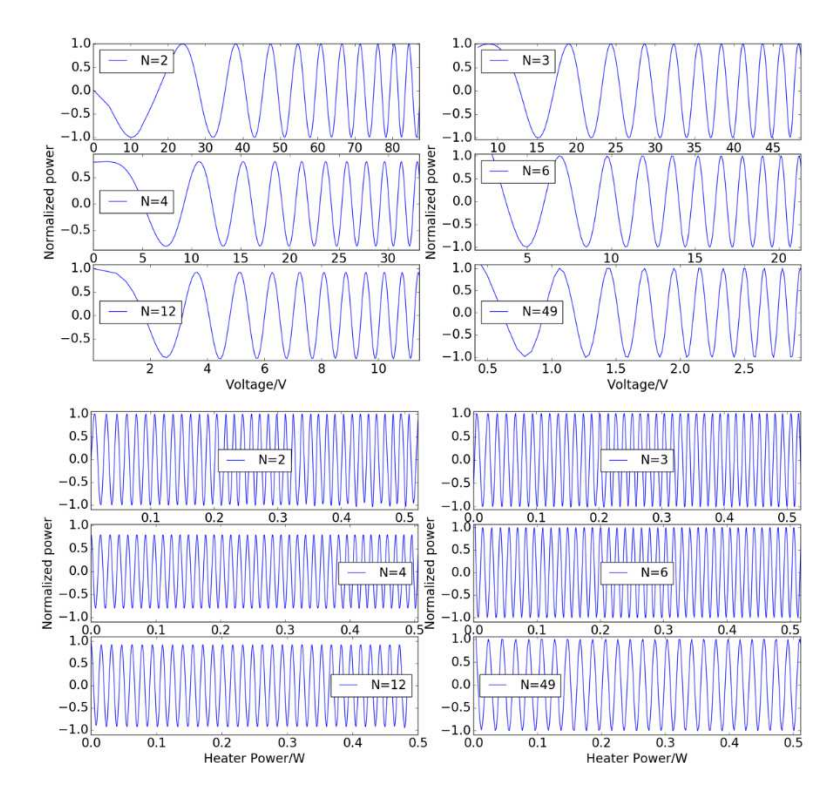


Fig. 4. Measured optical output at 1540 for all the devices by sweeping voltage applied to the heaters. Top panel shows the results with x-axis being the voltage while bottom panel plots with x-axis being power.

While on the other hand, the power efficiency shows a more complicated trend as a function of N. To characterize the power efficiency, we fit the results using following equations:

$$I = A\cos(\Delta \varphi + \varphi_0) = A\cos\left(\frac{2\pi}{\lambda_0} k_n h r_h \frac{L_w}{WL} P + \varphi_0\right)$$
$$= A\cos\left(\frac{2\pi}{\lambda_0} \kappa P + \varphi_0\right)$$
(5)

where  $\lambda_0$  is the operation wavelength and  $\kappa = k_n h r_h \frac{L_w}{WL} = \eta \frac{L_w}{WL}$  is the core coefficient that describes how the output intensity responds with power injection to the heater and  $\eta = k_n h r_h$  is a notation for all the other geometry-independent constants. We will show later that, some heaters exhibit strong thermal nonlinearities at high power injection regime, then  $\kappa$  should be modified to include higher order Taylor terms:

$$\kappa = \kappa_0 + \kappa_1 P \tag{6}$$

The commonly used term to characterize power efficiency  $P_{\pi}$  is now related with  $\kappa$  through following equation:

$$P_{\pi} = \frac{\lambda_0}{\kappa} = \frac{\lambda_0 WL}{\eta L_w} \tag{7}$$

One might feel strange at the first sight of this equation, as usually  $P_{\pi}$  should be independent on waveguide length. This is true when  $L_{w} = L$ , which is the common case for short waveguides and heaters.

Before fitting, we notice that the measured interferograms usually exhibit distortions instead of being smooth sinusoidal curve due to many reasons like mechanical instability of the setup, drift of the fibers, thermal expansion of the silicon chip as well as inaccuracy of the dc source. Thus, it is not wise to fit all the data (over hundreds of periods) simultaneously using equations Eq. (5)

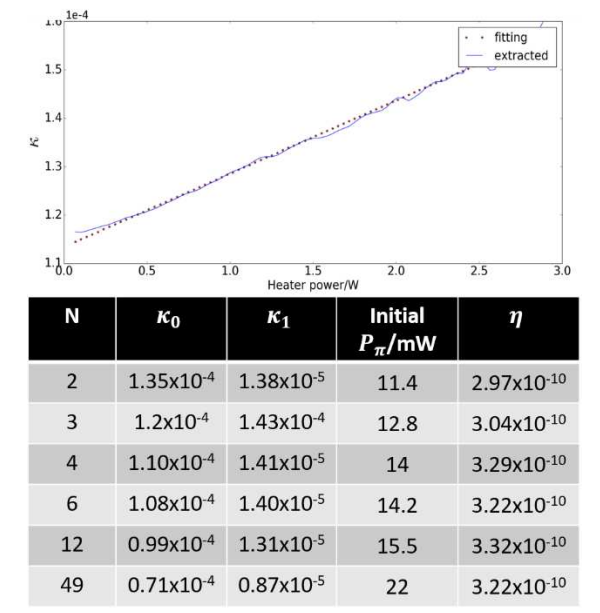


**Fig. 5.** An example of how we fit the measured results and the table with the extracted values of  $\kappa_0$ ,  $\kappa_1$  and initial  $P_{\pi} = \frac{\lambda_0}{\kappa_0}$  for each heater.

and Eq. (6). Instead, we use a moving window to fit a few periods each time using Eq. (5) and extract  $\kappa$  for each window. Then fit the collected series of  $\kappa$  using equation Eq. (6). A fitting example as well as the table containing extracted information of each heater are plotted in Fig. 5. There are a couple of issues to be discussed. First of all, it is quite clear that increasing N would lead to a drop of the power efficiency. But there is room for further optimization at large N. As in current design, the width of the center line of the heater (Fig. 1(b)) also increases with increasing N, which is unnecessary and would lead to a waste of power. For applications that require both high power efficiency and large phase change, there exists a tradeoff in the choice of N. Secondly, all heaters exhibit certain thermal nonlinearities with similar value except for N = 49, which shows minimal nonlinearities. Thermal nonlinearity has both advantages and disadvantages based on specific applications. On one hand, it would result in more phase change at high power level, which is beneficial for applications like spectrometers. On the other hand, it has to be carefully addressed for applications like tunable delay line and phase modulators. Thirdly, the coefficient  $\eta$  of each heater that combines all the material constants that are independent on the heater geometry have similar value, which is in consistent with the theory.

#### 4. Conclusion

In this paper, we characterize ultra-long integrated heaters through both theoretical modelling and experimental results. We propose a new design method for ultra-long heaters to retain compact footprint and achieve full-coverage of the waveguide. Our characterization provide design guidelines for applications with focus on maximum phase change with certain voltage and power consumption respectively. Moreover, the results confirm the existence of thermal nonlinearities of heaters.

**Funding.** National Key Research and Development Program of China (2021YFB2801500); Fast Support Program (80914010402); Natural Science Foundation of Jiangsu Province (BK20210288); National Natural Science Foundation of China (62105149); Fundamental Research Funds for the Central Universities (NS2022043).

**Disclosures.** The authors declare no conflicts of interest.

**Data Availability.** Data underlying the results presented in this paper are not publicly available at this time but may be obtained from the authors upon reasonable request.

#### References

- D. Pérez, I. Gasulla, J. Capmany, and R. A. Soref, "Reconfigurable lattice mesh designs for programmable photonic processors," Opt. Express 24(11), 12093–12106 (2016).
- C. Taddei, L. Zhuang, M. Hoekman, A. Leinse, R. Oldenbeuving, P. van Dijk, and C. Roeloffzen, "Fully reconfigurable coupled ring resonator-based bandpass filter for microwave signal processing," in *Microwave Photonics (MWP) and* the 2014 9th Asia-Pacific Microwave Photonics Conference (APMP) 2014 International Topical Meeting on, (IEEE, 2014), 44–47.
- 3. L. Zhuang, C. Zhu, B. Corcoran, M. Burla, C. G. Roeloffzen, A. Leinse, J. Schröder, and A. J. Lowery, "Sub-GHz-resolution C-band Nyquist-filtering interleaver on a high-index-contrast photonic integrated circuit," Opt. Express 24(6), 5715–5727 (2016).
- A. Li and W. Bogaerts, "Experimental demonstration of a single silicon ring resonator with an ultra-wide FSR and tuning range," Opt. Lett. 42(23), 4986–4989 (2017).
- L. Zhuang, C. G. Roeloffzen, M. Hoekman, K.-J. Boller, and A. J. Lowery, "Programmable photonic signal processor chip for radiofrequency applications," Optica 2(10), 854–859 (2015).
- X. Wang, L. Zhou, R. Li, J. Xie, L. Lu, K. Wu, and J. Chen, "Continuously tunable ultra-thin silicon waveguide optical delay line," Optica 4(5), 507–515 (2017).
- H. Qiu, F. Zhou, J. Qie, Y. Yao, X. Hu, Y. Zhang, X. Xiao, Y. Yu, J. Dong, and X. Zhang, "A continuously tunable sub-gigahertz microwave photonic bandpass filter based on an ultra-high-Q silicon microring resonator," J. Lightwave Technol. 36(19), 4312–4318 (2018).
- 8. M. C. Souza, A. Grieco, N. C. Frateschi, and Y. Fainman, "Fourier transform spectrometer on silicon with thermo-optic non-linearity and dispersion correction," Nat. Commun. 9(1), 665 (2018).
- A. Li and W. Bogaerts, "Using Backscattering and Backcoupling in Silicon Ring Resonators as a New Degree of Design Freedom," Laser Photonics Rev. 13, 1800244 (2019).
- X. Wu, T. Fan, A. A. Eftekhar, A. H. Hosseinnia, and A. Adibi, "High-Q ultrasensitive integrated photonic sensors based on slot-ring resonator on a 3C-SiC-on-insulator platform," Opt. Lett. 46(17), 4316–4319 (2021).

- 11. M. Corato-Zanarella, A. Gil-Molina, X. Ji, M. C. Shin, A. Mohanty, and M. Lipson, "Widely tunable and narrow linewidth chip-scale lasers from deep visible to near-IR," arXiv preprint arXiv:2109.08337 (2021).
- 12. A. Masood, M. Pantouvaki, G. Lepage, P. Verheyen, J. Van Campenhout, P. Absil, D. Van Thourhout, and W. Bogaerts, "Comparison of heater architectures for thermal control of silicon photonic circuits," in 10th International Conference on Group IV Photonics, (IEEE, 2013), 83–84.
- 13. P. Dong, W. Qian, H. Liang, R. Shafiiha, D. Feng, G. Li, J. E. Cunningham, A. V. Krishnamoorthy, and M. Asghari, "Thermally tunable silicon racetrack resonators with ultralow tuning power," Opt. Express 18(19), 20298–20304
- 14. A. Li and W. Bogaerts, "Backcoupling manipulation in silicon ring resonators," Photonics Res. 6(6), 620-629 (2018).
- 15. Q. Cheng, L. Y. Dai, N. C. Abrams, Y.-H. Hung, P. E. Morrissey, M. Glick, P. O'Brien, and K. Bergman, "Ultralow-crosstalk, strictly non-blocking microring-based optical switch," Photonics Res. 7(2), 155–161 (2019).
- 16. R. Konoike, K. Suzuki, S. Namiki, H. Kawashima, and K. Ikeda, "Ultra-compact silicon photonics switch with high-density thermo-optic heaters," Opt. Express 27(7), 10332–10342 (2019).
- 17. W. Zhang and J. Yao, "A silicon photonic integrated frequency-tunable microwave photonic bandpass filter," in 2017  ${\it International\ Topical\ Meeting\ on\ Microwave\ Photonics\ (MWP),\ (IEEE,\ 2017),\ 1-4.}$
- 18. Y. Xie, Z. Geng, L. Zhuang, M. Burla, C. Taddei, M. Hoekman, A. Leinse, C. G. Roeloffzen, K.-J. Boller, and A. J. Lowery, "Programmable optical processor chips: toward photonic RF filters with DSP-level flexibility and MHz-band selectivity," Nanophotonics 7(2), 421–454 (2017).
- 19. B. Wu, Y. Yu, J. Xiong, and X. Zhang, "Silicon integrated interferometric optical gyroscope," Sci. Rep. 8(1), 8766 (2018).
- 20. R. M. Krishna, A. Eftekhar, S. Lee, T. Fan, X. Wu, A. Hosseinnia, H. Wang, M. Swaminathan, and A. Adibi, "Polysilicon micro-heaters for resonance tuning in CMOS photonics," Opt. Lett. 47(5), 1097–1100 (2022).
- 21. X. Wu, T. Fan, A. A. Eftekhar, and A. Adibi, "High-Q microresonators integrated with microheaters on a 3C-SiC-oninsulator platform," Opt. Lett. 44(20), 4941-4944 (2019).
- 22. P. Dong, W. Qian, H. Liang, R. Shafiiha, N.-N. Feng, D. Feng, X. Zheng, A. V. Krishnamoorthy, and M. Asghari, "Low power and compact reconfigurable multiplexing devices based on silicon microring resonators," Opt. Express 18(10), 9852-9858 (2010).
- 23. T. M. Tritt, Thermal conductivity: theory, properties, and applications (Springer Science & Business Media, 2005).
- 24. Y. Shabany, Heat transfer: thermal management of electronics (CRC press, 2009).